ELSEVIER

Optical Materials 17 (2001) 445–451

OPTICAL Materials

www.elsevier.com/locate/optmat

Enhancement of Er^{3+} $^4I_{13/2}$ population in Y_2O_3 by energy transfer to Ce^{3+}

Christof Strohhöfer *, Albert Polman

FOM Institute for Atomic and Molecular Physics, Kruislaan 407, 1098 SJ Amsterdam, The Netherlands

Received 20 November 2000; received in revised form 15 March 2001; accepted 2 April 2001

Abstract

We report measurements of the energy transfer between Er^{3+} and Ce^{3+} in Y_2O_3. The transition between the Er^{3+} $^4I_{11/2}$ and $^4I_{13/2}$ excited states can be stimulated by energy transfer to Ce^{3+}, augmenting the population in the $^4I_{13/2}$ state at the expense of that in the $^4I_{11/2}$ state. Experiments were performed on Y_2O_3 planar waveguides doped with 0.2 at.% erbium and 0–0.42 at.% cerium by ion implantation. From measurements of Er^{3+} decay rates as a function of cerium concentration we derive an energy transfer rate constant of 1.3×10^{-18} cm^3/s. The efficiency of the energy transfer amounts to 0.47 at 0.42 at.% cerium. The energy transfer rate constant measured in Y_2O_3 is two times smaller for $Er^{3+} \rightarrow Ce^{3+}$ than that for $Er^{3+} \rightarrow Eu^{3+}$ in the same material.

PACS: 32.50.+d; 42.70.Hj; 42.82.Gw

Keywords: Erbuim; Cerium; Y_2O_3; Codoping; Erbium amplifier; Energy transfer

1. Introduction

Optical amplifiers in telecommunication networks make use of population inversion between the first excited ($^4I_{13/2}$) and ground ($^4I_{15/2}$) states of Er^{3+} to achieve amplification around 1540 nm (cf. Fig. 1). Population inversion is obtained by exciting the second excited state $^4I_{11/2}$ with 980 nm radiation, from where the ion relaxes to the $^4I_{13/2}$ level by interactions with matrix vibrations. To attain high population of the $^4I_{13/2}$ state, this non-radiative de-excitation route has to be efficient compared to the radiative transitions from the $^4I_{11/2}$ and $^4I_{13/2}$ levels to the ground state.

In many promising amplifier and laser materials this is not the case. Their phonon energies are low, therefore multiple phonons are required to bridge the energy gap between the $^4I_{11/2}$ and $^4I_{13/2}$ levels, making the de-excitation inefficient. This means that when Er^{3+} is excited with 980 nm radiation, a considerable amount of energy is stored in the second excited state, and is not available for stimulated emission from the $^4I_{13/2}$ level. The efficiency of the transition from the $^4I_{11/2}$ to the $^4I_{13/2}$ state can be improved by transferring the energy difference between the two levels to a suitable acceptor ion. This process has been shown for Ce^{3+} [1–5] and Eu^{3+} [6,7] in glasses and crystalline materials. It is not known, however, which of these ions acts as the most efficient acceptor in a given material.

* Corresponding author. Tel.: +31-20-6081234; fax: +31-20-6684106.

E-mail address: c.strohhofer@amolf.nl (C. Strohhöfer).

0925-3467/01/$ - see front matter
PII: S0925-3467(01)00103-3

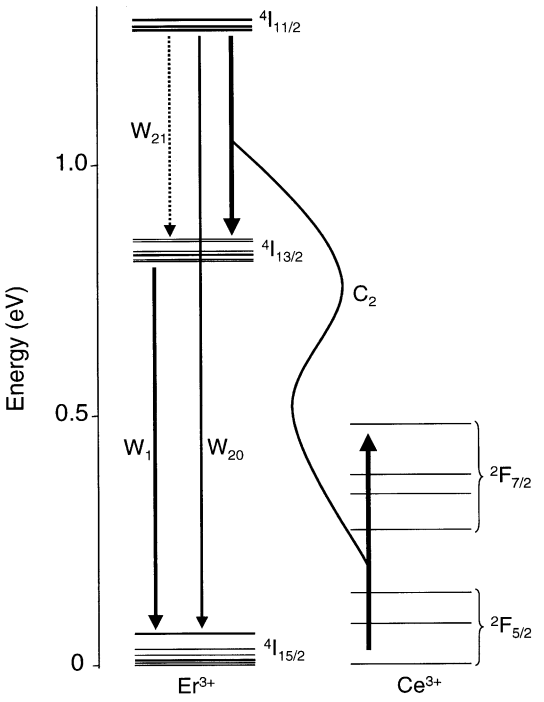

Fig. 1. Energy levels of Er^{3+} and Ce^{3+}. The arrows indicate the relevant transitions for the rate equation model.

In this article we describe codoping of Er^{3+}:Y_2O_3 with cerium. The choice of the host was suggested by its established properties as waveguide and amplifier material [8,9]. We are able to show that codoping with Ce^{3+} indeed increases the decay rate of the second excited state of Er^{3+} and the population in its first excited state. Comparing our present results to our data on the energy transfer between Er^{3+} and Eu^{3+} in Y_2O_3 [7], we show that the energy transfer efficiency between Er^{3+} and Ce^{3+} is lower by a factor of two.

2. Experimental

The yttrium oxide planar waveguides were fabricated by sputter deposition on thermally oxidised silicon wafers [8]. The SiO_2 and Y_2O_3 layer thicknesses are 3 μm and 750 nm, respectively, as determined with Rutherford backscattering spectrometry (RBS). To dope the Y_2O_3 with the rare earth ions we have used ion implantation, as it is known to lead to well controlled doping profiles and a homogeneous distribution of the implanted ions. These samples were implanted with erbium at energies between 200 and 500 keV to a total fluence of 1.34×10^{15} cm^{-2} to create a flat dopant profile at a concentration of 1.38×10^{20} cm^{-3} (0.21 at.%) over the depth from 30 to 130 nm from the surface. Cerium was then coimplanted into parts of the samples at energies between 185 and 425 keV. These energies were chosen such as to match the cerium and erbium dopant profiles. Nominal implantation fluences were 2.17×10^{14}, 6.9×10^{14}, 1.73×10^{15}, and 2.68×10^{15} cm^{-2}. The cerium concentrations were obtained by RBS and amount to 0.05, 0.07, 0.25, and 0.42 at.%. The sample temperature was kept at 77 K during all implantations. After ion implantation, the samples were annealed at 700°C for 1 h in a vacuum furnace at a base pressure below 10^{-4} Pa. The part of the samples not implanted with cerium serves as an on-wafer reference for the analysis. In this way slight differences in luminescent properties between the samples can be taken into account.

Room temperature photoluminescence from Er^{3+} was measured by exploiting the planar waveguide geometry of the samples. Light from an Ar^+ ion laser operating at 488 nm was mechanically chopped and butt-coupled into the samples using an optical fibre. The photo-luminescence emission from the different energy levels of Er^{3+} was collected perpendicular to the waveguide plane with an optical fibre of core diameter 0.8 mm. The light was dispersed in a 96 cm monochromator and detected with an AgOCs photomultiplier tube in the wavelength region between 500 and 1100 nm, and a germanium detector cooled to 77 K in the region around 1500 nm.

Photoluminescence decay traces of the Er^{3+} $^4I_{13/2}$ energy level at 1538 nm were recorded on a digital oscilloscope, averaging typically 2500 single traces for each measurement. The decay traces of the $^4I_{11/2}$ level at 980 nm as well as of the higher lying energy levels were measured using a photon counting system and a multichannel scaler. The decay traces were fitted by single exponential functions to obtain the decay rates. Only the decay of the $^4I_{11/2}$ level in the sample with the highest cerium concentration was not single exponential.

In this case the first e-folding time has been used to define the decay rate.

Values for the ratio of intensities emitted from the $^4I_{13/2}$ and $^4I_{11/2}$ states were obtained by measuring photoluminescence spectra of the corresponding emission lines under identical experimental conditions, using the Ge detector. The spectral resolution was set to 3 nm, the Er^{3+} was excited with 488 nm radiation. Standard lock-in techniques were employed to reduce the noise level. The spectra were corrected for the detector response and integrated in the frequency domain to obtain the emission intensity in each line.

For all the measurements reported in this article, care has been taken to keep the excitation power so low as to ensure a linear relationship between excitation and emission intensities. In this way, power and population dependent effects, like cooperative upconversion and excited state absorption, can be excluded and do not have to be taken into account for the analysis.

3. Results and discussion

3.1. Rate equation model

In Fig. 1 we show a schematic of the mechanism that accelerates the transition between the Er^{3+}, $^4I_{11/2}$ and $^4I_{13/2}$ states. The transition rates W_1, W_{20}, and W_{21} are defined as the intrinsic Er^{3+} rates in Y_2O_3. W_1 is the decay rate of the $^4I_{13/2}$ level and can be written as the sum of a radiative rate W_{1r} and a non-radiative rate W_{1nr}. W_{21} and W_{20} are the rates of the transitions from the $^4I_{11/2}$ level to the $^4I_{13/2}$ and $^4I_{15/2}$ states, respectively. We define W_{21} as the sum of the relevant radiative and non-radiative transition rates, while we assume W_{20} to be purely radiative. The sum of W_{21} and W_{20}, W_2, is the total decay rate of the $^4I_{11/2}$ level.

The coupling of the $^4I_{11/2} \rightarrow {}^4I_{13/2}$ transition with Ce^{3+} depends on cerium concentration and is described by the rate constant C_2. We assume the population in the $^2F_{7/2}$ state of Ce^{3+} to be negligible at all times. This presumption is plausible at room temperature, considering that the Stark levels of both the $^2F_{7/2}$ and $^2F_{5/2}$ energy levels are split widely in Y_2O_3 [10] and all energy gaps can be bridged by two to three phonons of the Y_2O_3 host (highest phonon density of states at 400 cm^{-1} [11]).

As described in detail in [7], to account for effects due to the ion implantation, we have to introduce an additional phenomenological decay rate of the Er^{3+} $^4I_{13/2}$ state, S_1. The interaction causing this decay can either be due to the presence of energy levels of Ce^{3+} (e.g., via phonon-assisted energy transfer) or to implantation defects. Taking further into account that the excitation of the Er^{3+} takes place into the $^4F_{7/2}$ state at 488 nm, the rate equations for the $^4I_{11/2}$ and $^4I_{13/2}$ levels can be written as

$$\begin{aligned} \frac{dN_2}{dt} &= R_2 - W_2N_2 - C_2N_qN_2, \\ \frac{dN_1}{dt} &= R_1 - W_1N_1 + W_{21}N_2 + C_2N_qN_2 - S_1N_1. \end{aligned} \tag{1}$$

The symbols R_1 and R_2 refer to the excitation rate per unit volume into the first and second excited states of Er^{3+} (as indicated by the subscripts). They depend on the branching ratio of the $^4F_{7/2}$ level and possibly lower states. N_1, N_2 are the population densities in the first and second excited states of Er^{3+}, and N_q refers to the codopant concentration. Implicit in these equations is the assumption that the excitation density is small enough to preclude bleaching of the ground state and nonlinear processes such as upconversion by energy transfer. These equations are easily adapted to describe excitation of the $^4I_{11/2}$ state by radiation around 980 nm. The only change necessary is setting $R_1 = 0$.

We can now define the fraction of the population in the $^4I_{11/2}$ level that is de-excited via energy transfer to Ce^{3+} as

$$Q_2 = \frac{C_2N_q}{W_2 + C_2N_q}. \tag{2}$$

The choice of this function, namely the linear dependence of the energy transfer rate C_qN_q on cerium concentration, is justified by experiment (cf. Section 3.2). Similarly we can write the fraction of population in the $^4I_{13/2}$ level that is de-excited due to the interaction S_1 as

$$Q_1 = \frac{S_1}{W_1 + S_1}. \tag{3}$$

These branching ratios serve as a measure for the efficiency of the de-excitation processes acting on the two energy levels and are determined by means of decay rate measurements.

To obtain an expression for the ratio of the emission intensities of the $^4I_{13/2}$ and $^4I_{11/2}$ levels, we substitute the expressions for Q_1 and Q_2 into the rate equation, Eq. (1). Expressing the emission intensities in terms of the population in each level, $I_1 = W_{1r} h\nu_1 N_1$ and $I_2 = W_{20} h\nu_2 N_2$, the intensity ratio can be written as

$$\frac{I_1}{I_2} = \frac{1 - Q_1}{1 - Q_2} \frac{I_1^0}{I_2^0} + \frac{W_{1r}}{W_1} \frac{Q_2(1 - Q_1)}{1 - Q_2} \frac{\nu_1}{\nu_2}, \tag{4}$$

where I_1 and I_2 are the integrated emission intensities pertaining to transitions from first and second excited state of Er^{3+} to its ground state in the presence of cerium, and I_1^0 and I_2^0 the intensities in the limit of zero cerium concentration. ν_1 and ν_2 are the corresponding emission frequencies. We assume that W_{20} is purely radiative.

3.2. Experimental results

Fig. 1 shows the energy levels for Er^{3+} and Ce^{3+} in Y_2O_3 as reported by Chang et al. [10]. The Stark levels of the Ce^{3+} $^2F_{7/2}$ and $^2F_{5/2}$ states are split widely and therefore provide for efficient de-excitation of the upper levels via vibrational interactions with the Y_2O_3 lattice. The transition between the lowest energy Stark level of the ground state and the highest energy Stark level of the excited state is resonant with the transition between the $^4I_{11/2}$ and $^4I_{13/2}$ levels of Er^{3+}. This is the condition necessary for active transfer of population from the $^4I_{11/2}$ to the $^4I_{13/2}$ state of Er^{3+} and thus for an increased transition rate between the $^4I_{11/2}$ and $^4I_{13/2}$ levels of Er^{3+}.

The interaction between Er^{3+} and Ce^{3+} manifests itself by an increased decay rate of the Er^{3+} $^4I_{11/2}$ level. The difference between the $^4I_{11/2}$ decay rates for cerium concentrations N_q and zero can be interpreted as the energy transfer rate from the Er^{3+}:$^4I_{11/2}$ state to cerium

$$W_{tr}^{N_q} = W_{981}^{N_q} - W_{981}^0 \tag{5}$$

with W_{981}^{0,N_q} the measured decay rates at cerium concentrations of zero and N_q. As shown in the inset of Fig. 2, a double logarithmic plot of W_{tr} against N_q, the transfer rate depends linearly on cerium concentration. This result justifies the definition of Eq. (2) as the efficiency of de-excitation via Ce^{3+}.

The energy transfer efficiency between Er^{3+} and Ce^{3+} can be derived from experimental data as

$$Q_{981}^{N_q} = 1 - \frac{W_{981}^0}{W_{981}^{N_q}} \tag{6}$$

and a similar definition can be given for the energy transfer efficiency from the Er^{3+} $^4I_{13/2}$ state, $Q_{1538}^{N_q}$.

The values obtained for both $Q_{981}^{N_q}$ and $Q_{1538}^{N_q}$ at different cerium concentrations are plotted in Fig. 2. Q_{981} rises monotonically over the full concentration range, reaching a value of 0.47 for 0.42 at.% cerium. This behaviour is expected when energy transfer from the Er^{3+} $^4I_{11/2}$ level to Ce^{3+} takes place. By fitting the data for Q_{981} with the function given by Eq. (2), we determine the energy transfer coefficient

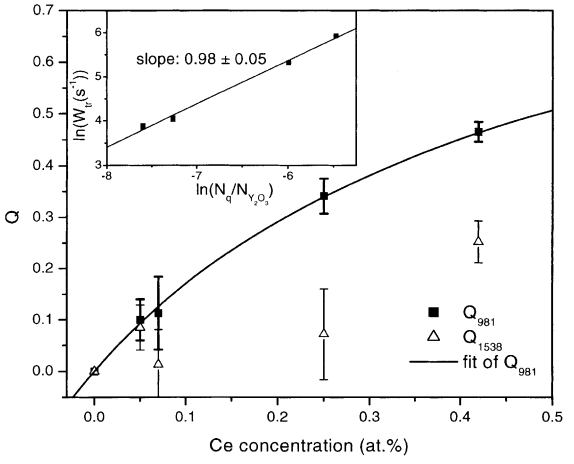

Fig. 2. Efficiency of the Er^{3+} ($^4I_{11/2} \rightarrow {}^4I_{13/2}$) to Ce^{3+} energy transfer (Q_{981}) and the fraction of energy lost from the Er^{3+} $^4I_{13/2}$ state due to cerium implantation (Q_{1538}). The line is a fit of Eq. (2) to the data for Q_{981}. The inset shows a double logarithmic plot of the transfer rate W_{tr} from the Er^{3+} $^4I_{11/2}$ state to cerium vs cerium concentration. The linear dependence justifies the definition of $W_{tr} = C_q N_q$ in Eq. (2).

C_2 to be $(1.3 \pm 0.1) \times 10^{-18}$ cm^3/s. Q_{1538} also increases with cerium concentration. The data cannot be described, however, by a function of the form of Eq. (2) and therefore by an energy transfer to cerium. Similar behaviour has been observed in previous work on the same system using Eu^{3+} as the codopant [7]. It is attributed to defects induced by the ion implantation that are not removed during the anneal of the samples.

The increase of the decay rate of the Er^{3+} $^4I_{11/2}$ state due to cerium codoping does of course also have an influence on the shape of the decay curves of the $^4I_{13/2}$ state. The $^4I_{13/2}$ state receives excitation from the $^4I_{11/2}$ state on the time scale of the $^4I_{11/2}$ decay rate W_{981}. This can be discerned in the $^4I_{13/2}$ decay at short times [12]. Fig. 3 compares the decay traces doped with 0 and 0.25 at.% cerium. While both traces approach the same decay rate at long times, initially there is a clear difference between them. When no codoping with cerium has taken place, the decay is clearly non-exponential at short times. It becomes more single exponential when cerium is introduced as codopant. Solving the rate Eq. (1), we obtain the decay function of the $^4I_{13/2}$ state as

$$N_1(t) = \left(N_1^0 + \frac{W_{21}N_2^0}{W_2 - W_1}\right)e^{-W_1 t} - \frac{W_{21}N_2^0}{W_2 - W_1}e^{-W_2 t}, \tag{7}$$

where N_1^0 and N_2^0 represent the initial population of the $^4I_{13/2}$ and $^4I_{11/2}$ manifolds.

It is clear that all information on the decay rates of the $^4I_{11/2}$ state is contained in the decay traces of the $^4I_{13/2}$ state. Fitting Eq. (7) to the decay trace without cerium (for data and fit cf. Fig. 3), we obtain a value of 392 ± 50 s^{-1} for W_2. It is in reasonable agreement with the one measured by direct observation of the decay of the $^4I_{11/2}$ level (428 ± 8 s^{-1}). The accuracy is however lower than for the direct measurement, and decreases even further when the decay rate W_2 increases.

Evidence that the population from the $^4I_{11/2}$ state of Er^{3+} is indeed transferred to the $^4I_{13/2}$ state is provided by measurements of the ratio between the photoluminescence intensities emitted from these two levels. These are plotted in Fig. 4. As expected from considerations of the model outlined in Fig. 1, the data show an increase of the intensity ratio of the $^4I_{13/2}$ and $^4I_{11/2}$ levels with increasing cerium concentration. This indicates that the population in the first excited state of Er^{3+} is growing with respect to the population in its

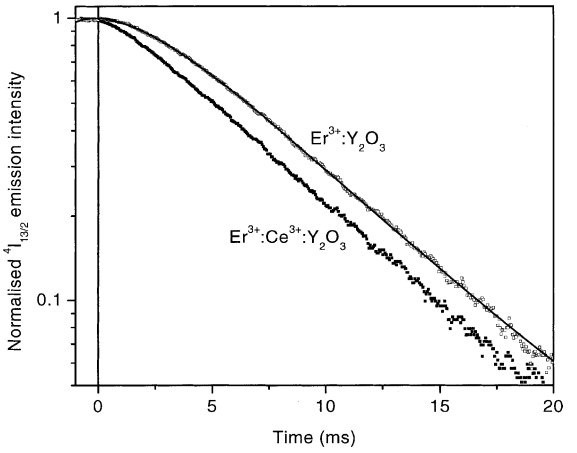

Fig. 3. Decay of the $^4I_{13/2}$ emission at 1538 nm for a sample containing only erbium and a sample codoped with 0.25 at.% cerium, excited at 488 nm. The decay at short times is slower than at long times, reflecting the de-excitation of the $^4I_{11/2}$ to the $^4I_{13/2}$ manifold. The drawn line is a fit of Eq. (7) to the data. Note that the effect decreases with cerium codoping, an indication of the increase in decay rate of the $^4I_{11/2}$ state.

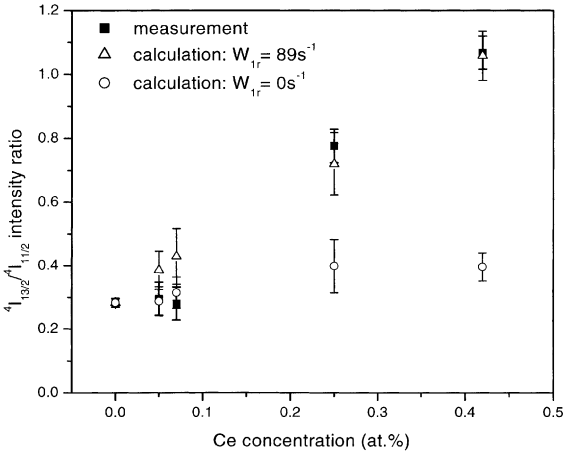

Fig. 4. Ratio of emission intensity from the Er^{3+} $^4I_{13/2}$ and $^4I_{11/2}$ energy levels. Overlaid is a calculation according to Eq. (4) with $W_{1r} = 89$ s^{-1}, using the data from Fig. 2. Direct de-excitation of the Er^{3+} $^4I_{11/2}$ state to the ground state ($W_{1r} = 0$) does not reproduce the data.

second excited state. Making use of the values for the Q_i's obtained from decay rate measurements (cf. Fig. 2), we can calculate the expected behaviour of the $^4I_{13/2}/^4I_{11/2}$ intensity ratio according to Eq. (4). The only free parameter in the calculation is the radiative decay rate of the $^4I_{13/2}$ level. The minimal mean squared deviation between data and calculation is achieved for $W_{1r} = 89\ s^{-1}$. Note that correspondence between calculation and experiment cannot be obtained assuming direct de-excitation of the $^4I_{11/2}$ level to the ground state. In this case the intensity ratio is determined completely by the measured decay rates, without any adjustable parameters. Mathematically this is equivalent to setting $W_{1r} = 0$ in Eq. (4). The values of the intensity ratio under this condition are also shown in Fig. 4.

3.3. Comparison of the effects of cerium and europium codoping

Let us briefly compare two results of this work with our previous measurements on Er^{3+} in Y_2O_3 codoped with europium [7]. For the case of codoping with europium we determined the energy transfer coefficient C_2 to be $2.9 \times 10^{-18}\ cm^3/s$, more than a factor of two higher than for codoping with cerium. According to Dexter [13], multipolar energy transfer depends on the overlap integral between donor emission and acceptor absorption. Comparing the energy level structure of Ce^{3+} and Eu^{3+} in Y_2O_3 [10,14] shows that the higher transfer efficiency towards Eu^{3+} is due to the better spectral overlap between the Er^{3+} $^4I_{11/2} \rightarrow {}^4I_{13/2}$ transition and the Eu^{3+} energy levels. Measurements in glasses of different compositions [4,5] suggest that energy transfer between Er^{3+} and Ce^{3+} contains a phonon-assisted contribution. A similar process is suggested by decay rate measurements at different temperatures on our samples. These are shown in Fig. 5. Plotted are the decay rates of the Er^{3+} $^4I_{11/2}$ state for a sample codoped with 0.25 at.% cerium and a reference without cerium. Both sets of decay rate measurements show an increase with temperature, due to phonon-assisted de-excitation to the $^4I_{13/2}$ state. The energy transfer rate W_{tr}, also drawn in Fig. 5, increases with temperature as well, by 60% over

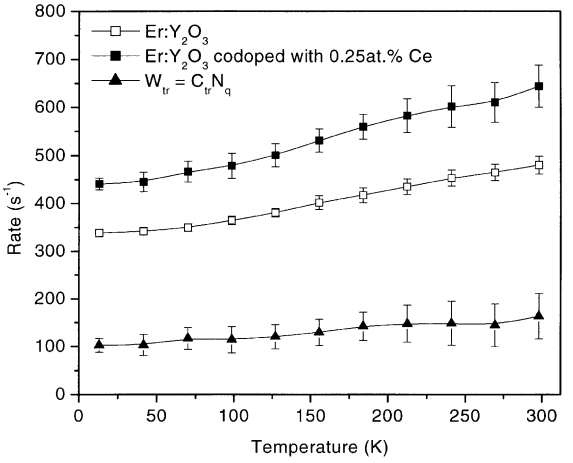

Fig. 5. Measured decay rates of Er^{3+} in samples with 0 and 0.25 at.% cerium as a function of temperature. The energy transfer rate W_{tr} from Er^{3+} to Ce^{3+} is derived from these measurements. The lines are drawn as guides to the eye.

the temperature range between 13 and 300 K. Since the energy transfer rate does not vanish at 13 K we can conclude that some direct energy transfer from Er^{3+} to Ce^{3+} takes place. Although the accuracy of these measurements is limited, the temperature dependence of W_{tr} suggests a considerable phonon-mediated component at room temperature. The poor overlap together with this phonon-assisted contribution can explain the lower efficiency for energy transfer between Er^{3+} and Ce^{3+}.

It is interesting to note the correspondence of the values for the adjustable parameter (W_{1r}) in the fit of Eq. (4) to the intensity ratio data for experiments involving different acceptor ions. It amounts to $89\ s^{-1}$ for both energy transfer between Er^{3+} and Eu^{3+} presented earlier [7] and energy transfer between Er^{3+} and Ce^{3+} described in this article. This fact supports the claim that all transitions from the $^4I_{11/2}$ state induced by the codopants have the $^4I_{13/2}$ level as their final state: if an interaction were present de-exciting part of the excitation in the $^4I_{11/2}$ state directly to the ground state, the value for the adjustable parameter obtained from the ratio of the $^4I_{13/2}/^4I_{11/2}$ intensities would depend on the strength of this interaction. The interaction strength in turn depends on the energy level structure of the codopant, and treat-

ment conditions. Both are different for the two sample series and should therefore lead to different values of W_{1r}. Since this is not the case, the dominant de-excitation of the $^4I_{11/2}$ state induced by the codopant must be to the $^4I_{13/2}$ level.

4. Conclusion

In this article we have shown that in a Y_2O_3 host the $^4I_{11/2} \rightarrow {}^4I_{13/2}$ transition in Er^{3+} can be accelerated by energy transfer to Ce^{3+}. In the process the population in the first excited state increases at the expense of the population in the second excited state. In this way the population inversion for amplification around 1540 nm is enhanced. This method is especially interesting for host materials with low phonon energies, whose steady-state population in the second excited state of Er^{3+} is high when excited with 980 nm radiation. In our experiments an energy transfer efficiency of 0.47 was measured for a cerium concentration of 0.42 at.%. The energy transfer coefficient was determined to be 1.3×10^{-18} cm^3/s.

The energy transfer between the $^4I_{11/2}$ state of Er^{3+} and Ce^{3+} in Y_2O_3 is less efficient than that between Er^{3+} and Eu^{3+}. This is attributed to the smaller spectral overlap of the Er^{3+} $^4I_{11/2} \rightarrow {}^4I_{13/2}$ transition with the absorption of the $^2F_{7/2}$ state of Ce^{3+}.

Acknowledgements

The authors would like to thank H.J. van Weerden and P.V. Lambeck from the University of Twente for providing the Y_2O_3 planar waveguides. This work is part of the research programme of the Dutch Foundation for Research on Matter (FOM) and was financially supported by NWO, IOP Electro-optics, and Symmorphix Inc.

References

[1] B. Simondi-Teisseire, B. Viana, D. Vivien, A.M. Lejus, Yb^{3+} to Er^{3+} energy transfer and rate-equations formalism in the eye safe laser material Yb:Er:$Ca_2Al_2SiO_7$, Opt. Mater. 6 (1996) 267.

[2] A.-F. Obaton, J. Bernard, C. Parent, G. Le Flem, C. Labbé, P. Le Boulanger, G. Boulon, Spectroscopic investigations of Yb^{3+}–Er^{3+}-codoped $LaLiP_4O_{12}$ glasses relevant for laser applications, Eur. Phys. J. Appl. Phys. 4 (1998) 315.

[3] Z. Meng, T. Yoshimura, Y. Nakata, N.J. Vasa, T. Okada, Improvement of fluorescence characteristics of Er^{3+}-doped fluoride glass by Ce^{3+} codoping, Jpn. J. Appl. Phys. 38 (1999) L1409.

[4] Z. Meng, T. Yoshimura, K. Fukue, M. Higashihata, Y. Nakata, T. Okada, Large improvement in quantum fluorescence yield of Er^{3+}-doped fluorozirconate and fluoroindate glasses by Ce^{3+} codoping, J. Appl. Phys. 88 (2000) 2187.

[5] Y.G. Choi, K.H. Kim, S.H. Park, J. Heo, Comparative study of energy transfers from Er^{3+} to Ce^{3+} in tellurite and sulfide glasses under 980 nm excitation, J. Appl. Phys. 88 (2000) 3832.

[6] A.A. Andronov, I.A. Grishin, V.A. Gur'ev, V.V. Orekhovskii, A.P. Savikin, Enhancement of the luminescence yield of Er^{3+} ions at $\lambda = 1.54$ μm in ZBLAN glass additionally doped with Er^{3+} and Tb^{3+} and pumped in the range $\lambda = 0.975$ μm, Tech. Phys. Lett. 24 (1998) 365.

[7] C. Strohhöfer, P.G. Kik, A. Polman, Selective modification of the Er^{3+} $^4I_{11/2}$ branching ratio by energy transfer to Er^{3+}, J. Appl. Phys. 88 (2000) 4486.

[8] T.H. Hoekstra, Erbium-doped Y_2O_3 integrated optical amplifiers, Ph.D. thesis, University of Twente, The Netherlands, 1994.

[9] H. van Weerden, T. Hoekstra, P. Lambeck, T. Popma, Low-threshold amplification at 1.5 μm in Er:Y_2O_3 IO-amplifier, in: Proceedings of the 8th European Conference on Integrated Optics, Stockholm, Sweden, Royal Institute of Technology, Stockholm, Sweden, 1997, p. 169.

[10] N.C. Chang, J.B. Gruber, R.P. Leavitt, C.A. Morrison, Optical spectra, energy levels, and crystal-field analysis of tripositive rate earth ions in Y_2O_3. I. Kramers ions in C_2 sites, J. Chem. Phys. 76 (1982) 3877.

[11] N. Yamada, S. Shionoya, T. Kushida, Phonon-assisted energy transfer between trivalent rare earth ions, J. Phys. Soc. Jpn. 32 (1972) 1577.

[12] J. Fick, É.J. Knystautas, A. Villeneuve, F. Schiettekatte, S. Roorda, K.A. Richardson, High photoluminescence in erbium-doped chalcogenide thin films, J. Non-Cryst. Solids 272 (2000) 200.

[13] D.L. Dexter, A theory of sensitized luminescence in solids, J. Chem. Phys. 21 (1953) 836.

[14] N.C. Chang, J.B. Gruber, Spectra and energy levels of Eu^{3+} in Y_2O_3, J. Chem. Phys. 41 (1964) 3227.